Journal of Magnetic Resonance 335 (2022) 107144

Contents lists available at ScienceDirect

Journal of Magnetic Resonance

journal homepage: www.elsevier.com/locate/jmr

Dynamic nuclear polarization-enhanced, double-quantum filtered ^{13}C-^{13}C dipolar correlation spectroscopy of natural ^{13}C abundant bone-tissue biomaterial

Sungsool Wi [a,*], Navneet Dwivedi [b,c], Richa Dubey [b], Frederic Mentink-Vigier [a], Neeraj Sinha [b,*]

[a] National High Magnetic Field Laboratory, Florida State University, Tallahassee, FL 32304, USA
[b] Department of Advanced Spectroscopy and Imaging, Centre of Biomedical Research, SGPGIMS Campus, Raebarelly Road, Lucknow 226014, India
[c] Department of Physics, Integral University, Lucknow 226026, India

ARTICLE INFO

Article history:
Received 3 October 2021
Revised 7 January 2022
Accepted 8 January 2022
Available online 13 January 2022

Keywords:
Natural 13C abundance protein
MAS DNP NMR
Solid-state NMR
Double-quantum Filter (DQF)
SPC-5
DARR
PDSD
AsymPolPOK

ABSTRACT

Here, we describe a method for obtaining a dynamic nuclear polarization (DNP)-enhanced double-quantum filtered (DQF) two-dimensional (2D) dipolar ^{13}C-^{13}C correlation spectra of bone-tissue material at natural ^{13}C abundance. DNP-enhanced DQF 2D dipolar ^{13}C-^{13}C spectra were obtained using a few different mixing times of the dipolar-assisted rotational resonance (DARR) scheme and these spectra were compared to a conventional 2D through-space double-quantum (DQ)-single-quantum (SQ) correlation spectrum. While this scheme can only be used for an assignment purpose to reveal the carbon-carbon connectivity within a residue, the DQF ^{13}C-^{13}C dipolar correlation scheme introduced here can be used to obtain longer distance carbon-carbon constraints. A DQF pulse block is placed before the DARR mixing scheme for removing dominant ^{13}C single-quantum (SQ) signals because these SQ ^{13}C signals are overwhelmingly large compared to those ^{13}C-^{13}C dipolar cross-peaks generated and therefore saturate the dynamic range of the NMR detection. This approach exhibits strong enough 2D cross-peaks in a dipolar ^{13}C-^{13}C correlation spectrum and potentially provides pairwise ^{13}C-^{13}C dipolar constraints because the dipolar truncation effect as well as multi-step signal propagations involving a spin cluster that contains more than two spins can be ignored probabilistically. To obtain fast signal averaging, AsymPolPOK was used to provide a short ^{1}H DNP signal build-up time (1.3 s) and to expedite our MAS DNP NMR acquisitions while still maintaining a satisfactory DNP enhancement factor ($\varepsilon = 50$). Under long DARR mixing, a t_1-noise-like artifact was observed at a site that possesses a large chemical shift anisotropy (CSA) and a few different strategies to address this problem were discussed.

1. Introduction

Bone is the natural composite biological tissue mainly composed of mineral phase and organic matrix. The organic matrix of bone mainly consists of type I collagen [1] which is structurally assembled in triple helical form. Due to the complicated heterogeneous structure of bone extracellular matrix (ECM), it is challenging for most of the biophysical techniques to analyze such system at atomistic level in their native state. Solid-state nuclear magnetic resonance (ssNMR) is a powerful and non-destructive technique capable of providing residue-specific structural information of such complex systems in their native state [2]. Magic-angle spinning (MAS) nuclear magnetic resonance (NMR) spectroscopy is used as an essential tool for determining the structure and dynamics of biosolids and materials. Combined with the Dynamic Nuclear Polarization (DNP) effect, it extends its scope further in these days as a powerful tool to detect so far non-observable signals by relying on the groundbreaking signal enhancement effect of DNP [3–9]. To conduct DNP-enhanced MAS NMR experiments on biological solids, biradical polarizing agents (PAs) (e.g. TOTAPOL [10] or AMUPOL [11]) are dissolved in water-based solvents at a few mM concentration and are thoroughly mixed with powdered solids of a sample under investigation to make this mixture form a "glassy state" at a low temperature ($\leq$100 K) [3,12–13]. The bis-nitroxide biradicals generate nuclear spin hyperpolarization via what is called the Cross-Effect mechanism [14–19]. This mechanism is particularly efficient under the MAS condition, as the time dependence induced by the rotation of sample generate energy level anti-crossings [17,20] called "rotor-events" [18,21–23]. The efficiency of the biradicals depends thus on the geometry of a rigid

* Corresponding authors.
E-mail address: sungsool@magnet.fsu.edu (S. Wi).

https://doi.org/10.1016/j.jmr.2022.107144
1090-7807/

molecular skeleton of a PA molecule and the distance between the two unpaired electron spins [18,21,24–27].

In majority of DNP-enhanced MAS NMR studies on biosolids, isotopically labeled samples with ^{13}C and/or ^{15}N have been employed as in conventional MAS NMR studies without DNP. In many cases however, it is possible to utilize natural ^{13}C or ^{15}N abundant samples to conduct NMR spectroscopy in solid state by relying on the signal enhancement effect of DNP. Indeed, a couple of types of MAS NMR experiments utilizing natural abundant ^{13}C or ^{15}N have been successfully conducted in the DNP-enhanced mode. For instance, in utilizing the natural abundant ^{13}C, the readily available types of experiments are the ^{1}H-^{13}C dipolar heteronuclear correlation (HETCOR) [28–29] or ^{13}C-^{13}C through-space DQ-SQ correlation spectroscopy [29–37]. However, the through-space DQ-SQ correlation scheme is not effective in detecting long-range ^{13}C-^{13}C distances. As a more advanced method, also attempted was a scheme for obtaining DNP-enhanced 2D ^{13}C-^{15}N correlations based on natural abundance ^{13}C and ^{15}N [38]. All these methods are efficient only for correlating short-range ^{1}H-^{13}C, ^{13}C-^{13}C, or ^{13}C-^{15}N dipolar pairs and are useful only for the peak assignment purposes. Also reported was a 2D ^{13}C-^{13}C correlation scheme based on the indirect ^{1}H-^{1}H mixing [39]. Since this method achieves ^{13}C-^{13}C correlations by going through three steps of ^{1}H-^{13}C CP processes, the resultant signal intensity becomes weaker and it does not apply to carbons that do not possess directly bonded ^{1}Hs.

2D dipolar ^{13}C-^{13}C correlation spectroscopy by utilizing proton-driven spin diffusion (PDSD) [40–42], DARR [43–44], or the derivative methods of DARR [45–49] has been widely used for the structural analysis of uniformly and/or selectively ^{13}C-labeled biosolids. If the same experimental scheme can be used for analyzing biosolids without isotopic enrichments while utilizing the signal amplification effect of the DNP, it will be a powerful method that can be employed for investigating the structures of biosolids at a "low cost". However, in a DNP-enhanced 2D dipolar ^{13}C-^{13}C correlation spectrum of a sample at natural ^{13}C abundance with the DARR mixing scheme, the signal intensities of isolated ^{13}C peaks (diagonal peaks) are about 100 times stronger than those ^{13}C-^{13}C dipolar correlated peaks (cross-peaks). Thus, those diagonal peaks can saturate the dynamic range of the NMR receiver while burying small cross-peaks that are needed for structural characterization in the noise level. Therefore, as was widely practiced in the liquid-state NMR spectroscopy [50–52], a DQF pulse block can be utilized for removing the dominant SQ ^{13}C signals that are not participating in forming DQ coherences in obtaining 2D dipolar ^{13}C-^{13}C correlations.

In this manuscript we have used a symmetry-based pulse scheme as a DQF pulse block to remove dominant ^{13}C SQ coherences before (or after) applying the DARR mixing scheme to obtain a DNP-enhanced 2D dipolar ^{13}C-^{13}C correlation spectrum of a bone tissue sample in natural ^{13}C abundance. Two different versions of pulse sequences that produce in principle the same quality in achieving DQF 2D dipolar ^{13}C-^{13}C correlation spectra have been considered: DQ filtering prior to t_1 evolution (DOPE) (Fig. 1a) and DQ filtering after ^{13}C-^{13}C mixing (DOAM) (Fig. 1b) [53–54]. For both schemes PDSD [40–42], DARR [43–44] and its variants [45–48], including the AL FRESCO [49], can be used as a ^{13}C-^{13}C mixing scheme while considering the MAS spinning rate incorporated as well as the rf pulse power requirement. So far, these DOPE and DOAM methods were used to remove background single-quantum ^{13}C signals contributed from the natural ^{13}C abundance when a uniformly or selectively ^{13}C-labeled biological sample system is considered for producing ^{13}C-^{13}C correlations [53]. Elkins *et al.* utilized the DOPE method for selectively detecting only the signals from ^{13}C-^{13}C pair while removing isolated ^{13}C signals in ω_1 dimension in MAS DNP NMR experiments to study protein-cholesterol interactions while employing selectively ^{13}C-labeled M_2 protein and cholesterol [54]. In our study we have explored the feasibility of employing this DOPE scheme for conducting DNP-enhanced DQF 2D dipolar ^{13}C-^{13}C correlation spectroscopy of a natural ^{13}C abundant biological sample. A great advantage of this approach is that all ^{13}C-^{13}C dipolar pairs expected from a natural ^{13}C abundant sample system commute with one another because these ^{13}C-^{13}C dipolar pairs are probabilistically isolated from one another. The reason is that the natural ^{13}C abundance is only 1.01 % and, therefore, the probability of forming a spin cluster involving three or more ^{13}C spins is negligible. Thus, the dipolar truncation effect [55] as well as a potential multi-step signal transfer mode based on the relayed fashion spanning over multiple spins can be ignored.

A bisnitroxide PA, AsymPolPOK, [56] was used. It is a water-soluble nitroxide biradical that possesses a strong electron-electron spin coupling that reduces the depolarization effect and generates short nuclear spin polarization build-up times [56–57] (1.1 s; Supporting material). Thus, by employing a short time for the signal build-up as well as a recycle delay, each t_1 slice can be co-added within < 2 s to expedite the overall MAS DNP NMR acquisitions while generating a significant enhancement factor, $\epsilon_{on/off} \approx 50$ at 14.1 T. MAS-DNP enhanced 2D dipolar ^{13}C-^{13}C correlation spectra of a natural ^{13}C abundant bone tissue sample with and without a DQF block by employing a variable length of the DARR mixing scheme were obtained. A through-space DQ-SQ correlation spectrum obtained by employing the same SPC-5 pulse block [58] as used in the DQF block of the DQF 2D dipolar ^{13}C-^{13}C correlation scheme was obtained and compared. A t_1-noise-like problem appearing in the 2D spectrum that occurs when a long DARR mixing time was employed was discussed, and a few different approaches that would remove or minimize this problem were discussed.

2. Experimental section

2.1. Sample preparation

All the experiments were performed on goat cortical femora bone (*Capra hircus*, 2–3 years old). The bone sample was cleaned of soft tissues, bone marrow, cartilages and small size flakes were obtained by filing the intact bone with the help of bistoury. About 60 mg of powdered bone tissue sample in natural ^{13}C abundance was mixed (soaked) with about 60 μL of 10 mM AsymPolPOK in 90% D_2O /10% H_2O in an Eppendorf tube, and the mixture was shaken thoroughly by using a Vortex mixer. Then, the sample mixture was transferred and packed into a 3.2 mm sapphire rotor that is closed with a Vespel® cap for MAS spinning at ~ 100 K for conducting MAS DNP NMR experiments.

2.2. Experimental parameters

The DNP-enhanced DQF 2D dipolar ^{13}C-^{13}C correlation NMR experiment was carried out by employing a 3.2 mm ^{1}H-^{13}C-^{15}N triple-resonance MAS DNP probe on a gyrotron-based 395 GHz/14.1 T DNP NMR spectrometer that is operational with a Bruker Avance-III console [8,60–60]. All these spectra were measured at the sample temperature of ~ 100 K while irradiating microwaves.

A ^{1}H DNP signal build-up time (= ^{1}H T_1 time) measured on our sample mixture was 1.1 s (Supplementary Fig. 1). While the microwave is continuously irradiated on the sample at around 8 W power at the probe base, a saturation recovery pulse sequence, $[90^{\circ}(^{1}H)\text{-}1\ ms]_n$ (n = 100) that is applied along the ^{1}H channel, is followed by a short delay time of 1.3 s for the signal build-up that is placed before starting the ^{1}H-^{13}C CP process. The DNP enhance-

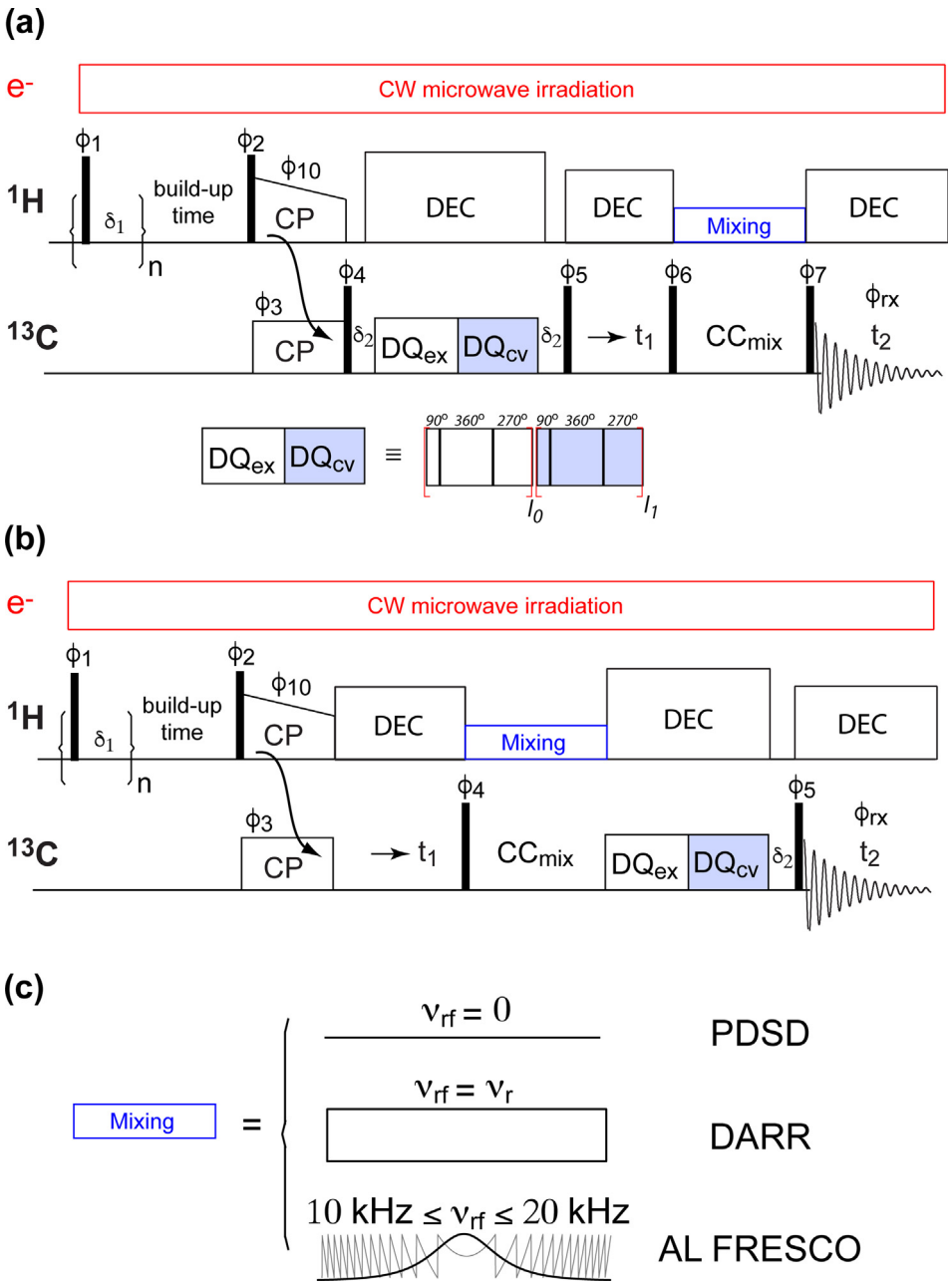

Fig. 1. The pulse sequences used for obtaining DNP-enhanced DQF dipolar ^{13}C-^{13}C correlation spectra employed in our study: (a) DOPE and (b) DOAM. Shown in Fig. 1c are examples of pulse blocks, such as PDSD, DARR or AL FRESCO, that can be employed as a ^{13}C-^{13}C mixing scheme in (a) and (b). The DQF pulse block can be placed before (a) or after (b) the 2D dipolar ^{13}C-^{13}C mixing block. We employed the SPC-5 sequence as a DQF pulse block although any other types of symmetry-based DQ generation sequences can be used depending on the MAS rate used. The pulse block in the gray color on the second half of the SPC-5 scheme that is employed for the conversion of DQ → SQ coherence is shifted in phase by 45-degrees every scan. The phase cycling routine of DOPE originally developed by Lopez et al. [53] was modified into a 32-step version to remove the undesirable axial peaks as well as the DC offset: $\phi_1 = \phi_3 = \phi_{10} = x$; $\phi_2 = (y)_4(-y)_4$; $\phi_4 = (-y)_4(y)_4$; $\phi_5 = (x)_8(-x)_8(y)_8(-y)_8$; $\phi_6 = (-y)_{16}(x)_{16}$; $\phi_7 = (x)_{16}(y)_{16}$; $\phi_{rx} = (x,-x)_4(-x,x)_4(y,-y)_4(-y,y)_4$. The phase cycling routine used for the DOAM sequence was: $\phi_1 = \phi_3 = \phi_{10} = x$; $\phi_2 = (y)_4(-y)_4$; $\phi_4 = (-y)_4(y)_4$; $\phi_5 = (x)_8(-x)_8(y)_8(-y)_8$; $\phi_{rx} = (x,-x)_4(-x,x)_4(y,-y)_4(-y,y)_4$. For both sequences in (a) and (b) the delay times δ_1 and δ_2 are 1 ms and $1/\nu_r$, respectively, where ν_r is the MAS rate.

ment factor measured by comparing the ^{1}H-^{13}C CPMAS spectra acquired with/without microwave irradiation was $\epsilon_{on/off} \approx 50$. The hyperpolarized proton magnetizations spreads over all ^{1}Hs in the sample system by spin diffusion before being transferred to ^{13}C magnetizations by ^{1}H-^{13}C cross-polarization (CP) [61–62]. Finally, magnetizations accrued along ^{13}Cs by CP are subject to proceed further to the pulse blocks of the DQF 2D ^{13}C-^{13}C dipolar correlation scheme as shown in Fig. 1. The ^{1}H and ^{13}C 90-degree pulse lengths used were 2.5 μs and 3.5 μs, respectively. A ^{1}H-^{13}C CP mixing scheme was applied for 1 ms that is formed by employing a ramped (90%-110%) spin-lock pulse along the ^{1}H channel centered at ν_{1H} = 60 kHz while simultaneously applying a rectangular spin-lock pulse of $\nu_{rf}[^{13}C]$ = 50 kHz along the ^{13}C channel. The MAS spinning rate was regulated at 8 kHz for satisfying $\nu_{rf}[^{13}C] = 5\nu_r = 40$ kHz for setting the SPC-5 pulse block for the DQF. During this SPC-5 block a non-excessive continuous wave (CW) ^{1}H decoupling power, $\nu_{rf}[^{1}H]$ = 105 kHz, was applied that is about 2.6 times greater than $\nu_{rf}[^{13}C]$ for SPC-5. The ^{1}H pulse power applied for the DARR mixing block was $\nu_{rf}[^{1}H] = \nu_r = 8$ kHz. For obtaining 2D ^{13}C-^{13}C correlations, 128–140 t_1 slices were acquired with an

acquisition delay time of 0.2 s by coadding 256, 384, and 512 scans for each t_1 slice while employing the DARR mixing time of 20 ms, 50 ms, and 100 ms, respectively. The SPINAL-64 sequence [63] with $\nu_{rf}[^1H]$ = 100 kHz was utilized as a ^1H decoupling scheme during both the t_1 and t_2 acquisition periods. In the present study, the chemical shift assignment (CcpNmr 2.5.2 version) and distance measurements (PyMOL) have been carried out using type-I collagen sequence (uniprot ID: CO1A1_BOVIN) [64] and spectrum is referenced with the distinctive Hyp C_γ resonances.

3. Results and discussion

Fig. 2 shows the comparison of the aliphatic regions of the DNP-enhanced 2D ^{13}C-^{13}C dipolar correlation spectra obtained by (a) the DARR mixing scheme without employing a DQF block, (b) the through-space DQ-SQ pulse scheme for producing a DQ-SQ correlation, and (c) the DARR mixing scheme with employing a DQF block. The DARR mixing time used in producing those spectra shown in Fig. 2a and 2c were both 50 ms, and the DQ excitation time and DQ → SQ reconversion time of the SPC-5 mixing sequence that were used as a DQF block (Fig. 2c) and as a through-space DQ-SQ mixing block (Fig. 2b) were $l_0 = l_1 = 10$ (=4/ν_r = 500 μs), which were found after optimization (see the Supplementary Fig. 2). In comparing those spectra shown in Fig. 2a and 2c, although these spectra were measured under the same DNP enhancement effect ($\epsilon_{on/off} \approx 50$) as well as under the same DARR mixing time (50 ms), while the conventional DARR spectrum obtained without DQF scheme does not produce any visible 2D cross-peaks, the DQF DARR spectrum does produce cross-peaks. This is because the dominant SQ ^{13}C peaks (diagonal) are about two orders of magnitude larger than ^{13}C-^{13}C cross-peaks and saturate the dynamic range of the signal receiver making the weak ^{13}C-^{13}C cross-peaks buried in the noise level and undetectable without DQF. Those stronger SQ ^{13}C peaks are filtered out with DQF and, therefore, those weaker 2D cross-peaks can be exhibited clearly as shown in Fig. 2c. Under the action of this DQF block, only those ^{13}C sites that possess at least an immediately adjacent (mainly directly bonded) ^{13}C site would form DQ coherences. Then, these DQ coherences are selected and reconverted back into SQ coherences by DQF, and these survived coherences are sent to the DARR mixing scheme for forming SQ-SQ ^{13}C-^{13}C correlations.

Although those ^{13}C sites survived from the DQF block are mostly from short-distance ^{13}C-^{13}C correlations that are formed between directly bonded pairs, long-distance^{13}C-^{13}C dipolar correlations can be formed among these sites in the following DARR mixing scheme in addition to those short-distance ^{13}C-^{13}C correlations depending on the length of the DARR mixing time employed. In a natural ^{13}C abundant sample system the probability of possessing a dipolar network that consists of more than 3 ^{13}C spins simultaneously is extremely low ($\leq 10^{-6}$). Therefore, each cross-peak appearing in the 2D DQF ^{13}C-^{13}C dipolar correlation spectrum measured would be generated from an isolated two-body ^{13}C-^{13}C spin pair that becomes easily detectable by the signal enhancement effect of DNP, and it is expected that a ^{13}C-^{13}C spin pair detected in a 2D DQF DARR spectrum would commute with any other ^{13}C-^{13}C pairs.

In a conventional through-space 2D DQ-SQ correlation spectrum (Fig. 2b) on a natural ^{13}C abundant sample, those DQ-SQ correlations do not suffer from the interference of dominant SQ ^{13}C coherences. For this reason, together with the 2D ^1H-^{13}C HETCOR, this has been a method of choice in MAS DNP NMR for investigating a natural ^{13}C abundant sample. Unfortunately, ^{13}C-^{13}C correlations found in those DQ-SQ correlation spectrum arise mostly from directly bonded ^{13}C-^{13}C pairs, and it is difficult to obtain long-range distance ^{13}C-^{13}C pair correlations because, as shown in the

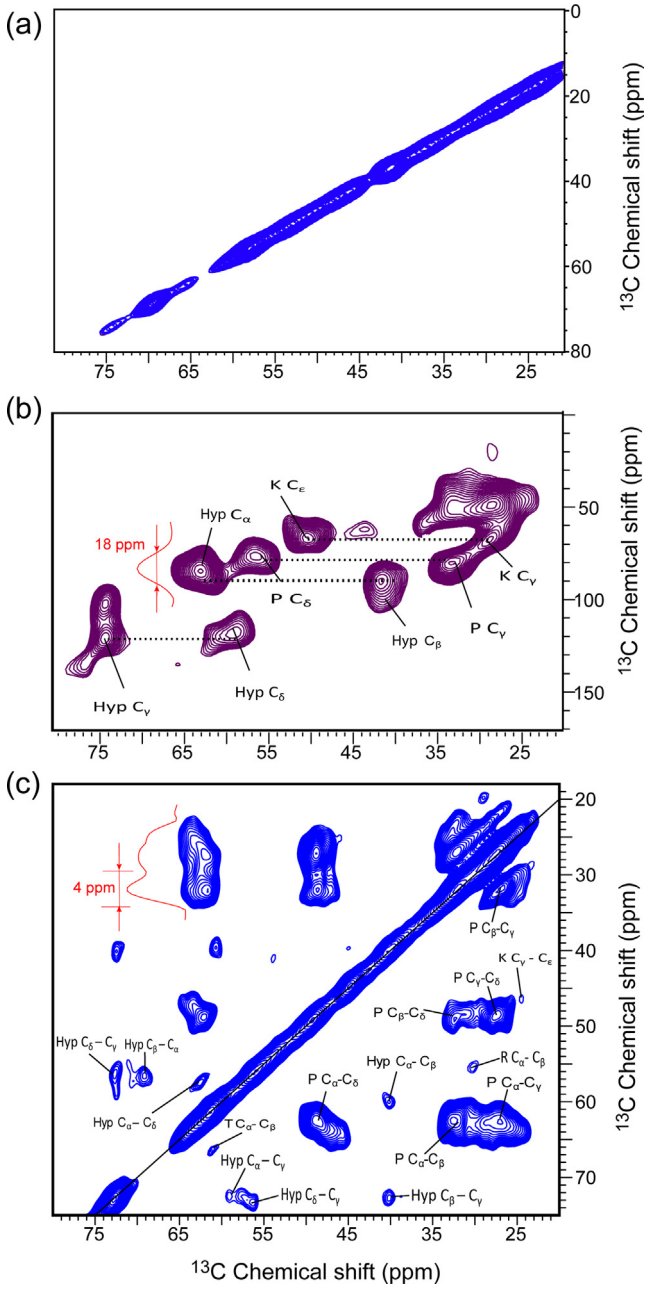

Fig. 2. 2D dipolar ^{13}C-^{13}C correlation spectra of goat cortical femora bone obtained without a DQF block (a) and with a DQF block (c). The spectrum shown in Fig. 2c was obtained by using the DOPE sequence as shown in Fig. 1a. An identical DARR mixing scheme possessing the same mixing time (50 ms) was used in both cases for obtaining ^{13}C-^{13}C correlations. The mixing time of both DQ excitation as well as the DQ → SQ reconversion of the SPC-5 pulse block employed in 2c was $l_0 = l_1 = 10$ (500 μs) that was found via optimization. The spectrum shown in Fig. 2b is the ^{13}C-^{13}C through-space DQ-SQ correlation spectrum obtained by employing the same SPC-5 pulse block as that used for the DQF block in 2c.

Supplementary Fig. 2, those ^{13}C signals decay rapidly during the SPC-5 block as the length of the mixing increases. In the case of the DQ-SQ correlation schemes, a symmetry-based rf pulse train is applied for the mixing time and signals undergo $T_1\rho$ relaxations that are normally shorter than T_1 relaxations and an accumulation of any potential rf pulse imperfections may lead to an additional signal decay. Moreover, the spectral resolution of a DQ-SQ correlation spectrum along the F_1 domain is lowered because the DQ mode signals decay faster than the SQ mode signals. Fig. 2b and 2c shows the projection peaks of a typical 2D peak [(F_2: 58 ppm,

F_1: 86 ppm) for 2b; (F_2: 62 ppm, F_1: 32 ppm) for 2c] obtained along the F_1 domain. In the processing of these spectra, an identical line-broadening window function was applied along the F_1 domain (Gaussian window function; line broadening (LB) = -30 Hz; Gaussian maximum position = 0.05). The linewidths of the DQ spectrum from the DQ-SQ scheme and the SQ spectrum from the DQF-DARR thus obtained were 18 ppm and 4 ppm, respectively, and it clearly demonstrates the superiority of the DQF-DARR over the DQ-SQ correlation scheme in obtaining a sharper peak along the indirect domain. Thus, the DARR mixing scheme is more powerful in providing better signal resolutions. Those cross-peaks visible in Fig. 2c arise from ^{13}C sites that are in close contact as a relatively short DARR mixing time (50 ms) was used, and therefore any noticeable long-range ^{13}C-^{13}C correlations are not significant. Thus, comparing spectra shown in Fig. 2b and 2c, most of the ^{13}C sites that exhibit cross-peak correlations in the DQF ^{13}C-^{13}C correlation spectrum are also visible in the 2D DQ-SQ correlation spectrum.

Fig. 3a and 3b show 2D DQF ^{13}C-^{13}C spectra measured by varying the length of the DARR mixing time by 20 ms and 100 ms, respectively. In all cases, the length of the DQF block employed is identical to $l_0 = l_1 = 10$, as used in Fig. 2b and 2c, which corresponds to 500 μs mixing time. As was discussed above and can be seen from Fig. 3a and 2c, when the DARR mixing time is relatively short (20–50 ms) most of the cross peaks seen in the spectra are from directly bonded short ^{13}C-^{13}C pairs. Indeed, not only the relative peak intensity of the cross-peaks produced at shorter mixing times has increased, but the occurrence of additional cross-peaks generated from longer distance ^{13}C-^{13}C pairs is evident as the DARR mixing time is increased.

It has been known that the organic component of bone matrix contains majority of type 1 collagen (nearly 90%) [65]. In this study also, most of the observed ^{13}C signals in 2D ^{13}C-^{13}C DAAR of goat cortical femora bone originate from type 1 collagen. Specifically, proline (P; ~28% of type 1 collagen), and hydroxyproline (Hyp; ~38% of type 1 collagen) [66] were majorly found inside the bone matrix. In the present study also, we observed the intra-residue correlation of Proline (1.5–2.4 Å), Hydroxyproline (1.5 Å) in the 2D ^{13}C-^{13}C DARR spectrum (20 ms and 50 ms) (Fig. 3a and 2b). Along with these, the additional correlations of the certain spin-systems such as Threonine (T) (1.5–2.6 Å), and Lysine (K) (2.4 Å) were also observed (Fig. 3a). With a longer DARR mixing time of 100 ms (Fig. 3b) additional cross-peaks (inter-residue correlations) are visible from further apart ^{13}C-^{13}C correlations (4.2–8.3 Å) as in the conventional case of applying the DARR mixing scheme to a uniformly or extensively ^{13}C-labeled sample system (2–10 Å) [67]. In the current study, we obtained the inter-residual cross peaks of spin systems such as T C_γ- L C_β, T C_γ- L C_γ, Hyp C_γ- A C_α, Hyp C_β- A C_α, and Hyp C_γ- P C_α in 2D ^{13}C-^{13}C DARR (100 ms) (Fig. 3b).

A t_1-noise-like issue was discovered as can be seen clearly by inspecting the full region of 2D DQF ^{13}C-^{13}C correlation spectra as shown in Supplementary Fig. 3a and 3b (20 ms and 100 ms). As can be seen in these spectra, this t_1-noise-like artifact is very intense under a longer DARR mixing (100 ms) at ^{13}C′ peaks that possess large chemical shift anisotropies (CSAs). Since the intensity of the cross-peak generated from an isolated ^{13}C-^{13}C pair that occurs at low probability (10^{-4}) is relatively weak even under the signal amplification of DNP, and there are no added signals propagated from other adjacent spins or spin clusters by a relayed fashion, the overall signal intensity of the cross-peak from a ^{13}C-^{13}C pair decreases sharply in inverse proportion to the third power of ^{13}C-^{13}C distance, approaching fast to the noise level of the spectrum. Thus, when a long-range ^{13}C-^{13}C pair is considered under a long DARR mixing time, a signal averaging must be performed with at least a few hundreds of scans coadded. The weak signal intensity of its barely surviving DQF signals can potentially start to interfere with the fluctuation level of the noise from scan to scan in the 2D acquisition when a lot of transient signals must be coadded for each t_1 slice. A careful investigation of these t_1-noise-like features reveals a rather regular pattern rather than a purely random form whose origin is not clearly understood at present. However, we speculate that this phenomenon might have a relationship with the CSA of the site that experiences an insufficient MAS averaging effect. Because a relatively low MAS rate (8 kHz) was employed compared to the size of the chemical shift anisotropy (CSA) of each C′ site, the peak of each C′ site is divided into a center-band and a few spinning sidebands for the MAS rate fails to average out CSA. As a result, the intensity of each divided and weakened MAS signal band is more likely to approach to and contend with the noise level. In addition to this, a signal reduction due to T_1 relaxation under a long longitudinal dipolar mixing time may also contribute to exacerbate the t_1-noise problem. This t_1-noise-like issue may be improved by confining it into the center-band by speeding up the MAS rate, but it should be noted that in speeding up MAS rate in DNP other considerations are present. In addition to reducing the size of the MAS rotor incorporated, these include the allowance of the probe for the strength of the ^{13}C rf pulse power (ν_{rf}^{13C}) of the DQF block (in the case of employing SPC-5 sequence it is $\nu_{rf}^{13C} = 5\ \nu_r$, where ν_r is the MAS rate) and the associated ^{1}H rf pulse power employed for the ^{1}H decoupling during this period that must be at least 2.3 times that of ν_{rf}^{13C}. In future experiments a faster MAS rate will be employed while employing the AL FRESCO type of mixing [49] by using a MAS DNP probe that incorporates a smaller MAS rotor size such as 1.9 mm or 1.3 mm. Moreover, a recently developed symmetry-based pulse technique can be employed as a DQF block that adopts a weaker ^{1}H decoupling power [68].

AMUPOL has given the largest enhancement factor among polarizing agents known ($\varepsilon = 160 - 247$) while employing glycerol-d_8 in the solvent system (typically 10 mM AMUPOL in 60% glycerol-d_8/ 30% D_2O/ 10% H_2O) [11,69–72]. However, the enhancement factor observed in our experiments by using 10 mM AMUPOL in 90% D_2O/10% H_2O was up to ~30. Because of its long DNP signal build-up time that normally takes ~ 3.5 s in the case of employing AMUPOL [11,70–70], the recycling of the signal acquisition takes a considerably longer time than that of using the AsymPolPOK whose optimal signal build-up time can be given within 1.3 s. Thus, together with the DNP signal enhancement factor obtained in this work of 50, it is more advantageous to use AsymPolPOK over AMUPOL to expedite the DNP experiments and achieves a better overall signal gain.

In addition to the DARR mixing scheme, it is expected that any variant methods of the DARR, such as PARIS-xy [45], SHANGHAI [46], CORD [48], AL FRESCO [49] etc., can also be used as a mixing scheme depending on the MAS rate employed. Particularly, the AL FRESCO scheme can be used effectively at any MAS rate as it employs a chirp pulse mixing scheme that requires a weak ^{1}H rf pulse power during the dipolar ^{13}C-^{13}C mixing period regardless of the speed of the MAS rate. The simplest mixing scheme, proton-driven spin diffusion (PDSD), will also be an efficient method since it deals with dilute ^{13}C spins particularly under employing a slow MAS rate (≤12 kHz) (see the Supporting Information). We have found that the PDSD mixing scheme also produces a t_1-noise-like issue, indicating that the applied ^{1}H rf pulse is not associated with the t_1-noise artifact. As a follow-up of this paper, we will examine how to solve this t_1-noise artifact with a few different options including the synchronization of the t_1-increment to the MAS rotor spinning. We believe that the experimental scheme presented in this paper has a potential to be employed economically in structural biology because it can be used directly for the structural analysis of proteins without iso-

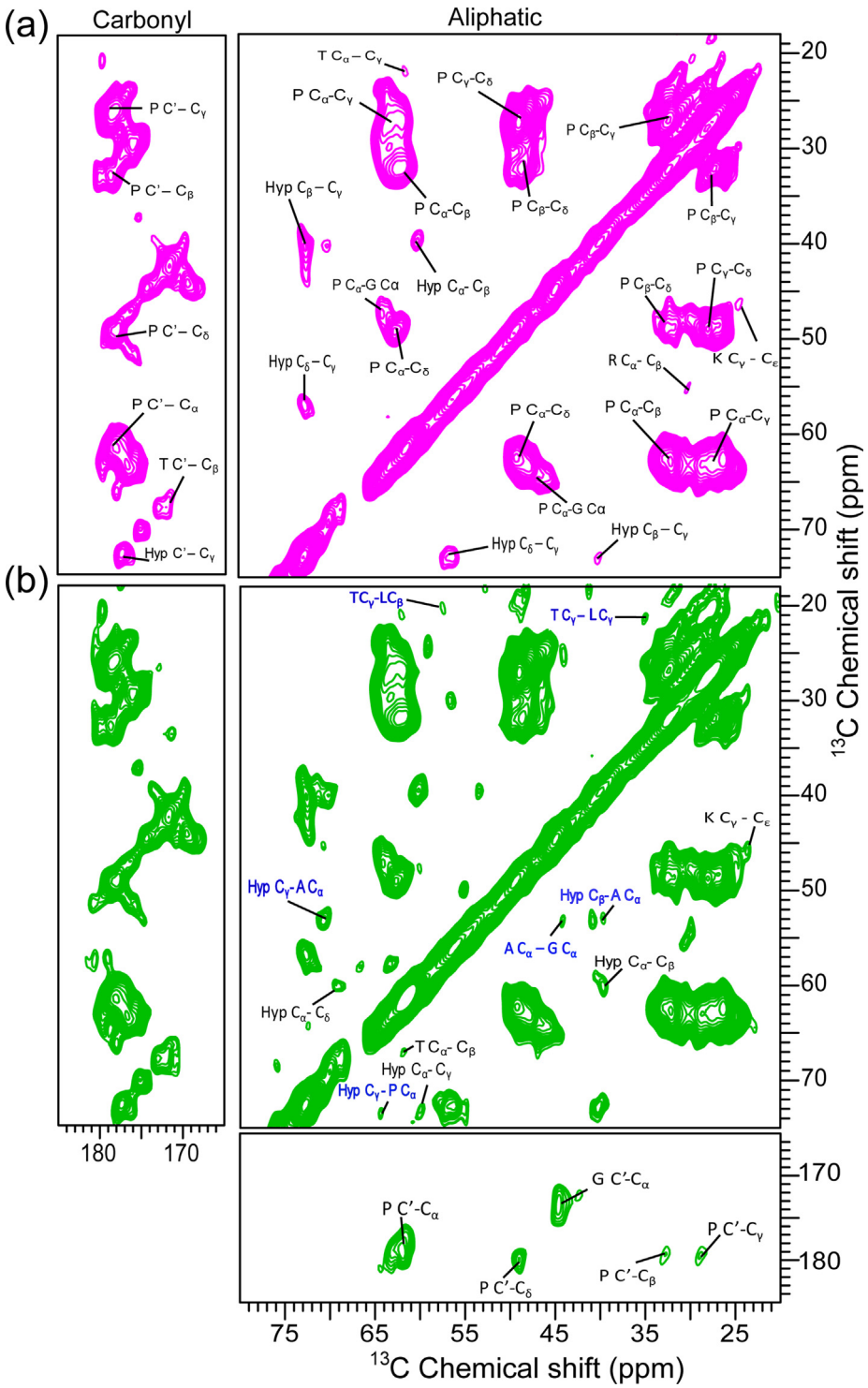

Fig. 3. DNP-enhanced DQF 2D dipolar ^{13}C-^{13}C correlation spectra of goat cortical femora bone obtained by employing the DOPE sequence with variable DARR mixing times of (a) 20 ms, (b) 100 ms. In all these cases, an identical type of SPC-5 pulse scheme was used as a DQF block as explained in the caption of Fig. 2. Under a short DARR mixing time (a), those ^{13}C-^{13}C cross-peak correlations detected are mostly from directly bonded ^{13}C-^{13}C pairs that are also evident in the DQ-SQ correlations exhibited in the spectrum as shown in Fig. 2b. However, in the case of employing a longer DARR mixing time (b), ^{13}C-^{13}C correlations from longer distances begin to appear. Only the spectral region that shows aliphatic-aliphatic correlations is presented. The intra-residue and inter-residue correlations were denoted in black and blue color respectively. Supplementary Fig. 3 shows the full regions of the spectra. (The one-letter codes for different amino acids are as following, T: Threonine, I: Isoleucine, K: Lysine, A: Alanine, G: Glycine, Hyp: Hydroxyproline, R: Arginine, P: Proline).

topic substitution, particularly for the proteins produced in mammalian cells, where isotope substitution is impossible or demanding.

Because the DARR mixing unit in the DQF-DARR scheme is not different from the conventional DARR mixing, the maximum ^{13}C-^{13}C distance the DQF-DARR scheme can provide would be the same as that from the conventional DARR or its derivative methods; it is known that the maximum ^{13}C-^{13}C distance the DARR or its derivative schemes can provide is about 7–9 Å when considered on a selectively ^{13}C labeled sample system [47]. However, an actual

experimental determination of the maximum ^{13}C-^{13}C distance the DQF-DARR scheme can afford would be challenging because of the poor signal-to-noise (S/N) ratio even under the DNP condition. When a small molecule system that is not ^{13}C-labeled is utilized, a contribution from the intermolecular ^{13}C-^{13}C contacts cannot be excluded due to having no means of sample dilution. An additional experimental challenge is that as the number of scans increases the range of ^{13}C-^{13}C distances that can be measured accurately with confidence would be extended as the S/N ratio is improved, but at the same time, a sweet period of the total experimental time should be determined by finding a counterbalance while considering the stability of the MAS DNP experimental conditions over time. Practically, an ideal sample system for this experiment should be a selectively ^{13}C-labeled model peptide or protein sample system of known structure.

Declaration of Competing Interest

The authors declare that they have no known competing financial interests or personal relationships that could have appeared to influence the work reported in this paper.

Acknowledgment

A portion of this work was performed at the National High Magnetic Field Laboratory, which is supported by the National Science Foundation Cooperative Agreement No. DMR-1644779 and the state of Florida, the MAS-DNP instrument is supported by the NIH P41 GM122698 and NIH S10 OD018519. S.W. thanks Thomas Halbritter and Snorri Th. Sigurdsson for supplying AsymPolPOK. N.D. acknowledges financial assistance from the Department of Science & Technology (DST), Government of India. R.D. is thankful for financial assistance from the Centre of Biomedical Research, SGPGI Campus Lucknow. N.S. acknowledges funding from CBMR, Lucknow.

Appendix A. Supplementary material

Supplementary data to this article can be found online at https://doi.org/10.1016/j.jmr.2022.107144.

References

[1] K. Grandfield, V. Vuong, H.P. Schwarcz, Ultrastructure of bone: hierarchical features from nanometer to micrometer scale revealed in focused ion beam sections in the TEM, Calcif. Tissue Int. 103 (2018) 606–616.
[2] I. Goldberga, R. Li, M.J. Duer, Collagen structure–function relationships from solid-state NMR spectroscopy, Acc. Chem. Res. 51 (2018) 1621–1629.
[3] D.A. Hall, D.C. Maus, G.J. Gerfen, S.J. Inati, L.R. Becerra, F.W. Dahlquist, R.G. Griffin, Polarization-enhanced NMR spectroscopy of biomolecules in frozen solution, Science 276 (1997) 930–932.
[4] Q.Z. Ni, E. Daviso, T.V. Can, E. Markhasin, S.K. Jawla, T.M. Swager, R.J. Temkin, J. Herzfeld, R.G. Griffin, High Frequency dynamic nuclear polarization, Acc. Chem. Res. 46 (2013) 1933–1941.
[5] A.J. Rossini, A. Zagdoun, M. Lelli, A. Lesage, C. Copéret, L. Emsley, Dynamic nuclear polarization surface enhanced NMR spectroscopy, Acc. Chem. Res. 46 (2013) 1942–1951.
[6] D. Lee, S. Hediger, G. De Paepe, Is solid-state NMR enhanced by dynamic nuclear polarization?, Solid State Nucl Magn. Reson. 66–67 (2015) 6–20.
[7] W. Zhai, A.L. Paioni, X. Cai, S. Narasimhan, J. Medeiros-Silva, W. Zhang, A. Rockenbauer, M. Weingarth, Y. Song, M. Baldus, Y. Liu, Postmodification via thiol-click chemistry yields hydrophilic trityl-nitroxide biradicals for biomolecular high-field dynamic nuclear polarization, J. Phys. Chem. B 124 (2020) 9047–9060.
[8] M. Rosay, L. Tometich, S. Pawsey, R. Bader, R. Schauwecker, M. Blank, P.M. Borchard, S.R. Cauffman, K.L. Felch, R.T. Weber, R.J. Temkin, R.G. Griffin, W.E. Maas, Solid-state dynamic nuclear polarization at 263 GHz: spectrometer design and experimental results, Phys. Chem. Chem. Phys. 12 (2010) 5850–5860.
[9] T.V. Can, Q.G. Ni, R.G. Griffin, Mechanisms of dynamic nuclear polarization in insulating solids, J. Magn. Reson. 253 (2015) 23–35.
[10] C. Song, K.-N. Hu, C.-G.-G. Joo, T.M. Swager, R.G. Griffin, TOTAPOL: A biradical polarizing agent for dynamic nuclear polarization experiments in aqueous media, J. Am. Chem. Soc. 128 (2006) 11385–11390.
[11] C. Sauvée, M. Rosay, G. Casano, F. Aussenac, R.T. Weber, O. Ouari, P. Tordo, Highly efficient, water-soluble polarizing agents for dynamic nuclear polarization at high frequency, Angew. Chemie Int. Ed. 52 (2013) 10858–10861.
[12] A.G.M. Rankin, J. Trébosc, F. Pourpoint, J.-P. Amoureux, O. Lafon, Recent developments in MAS DNP-NMR of materials, Solid State Nucl. Magn. Reson. 101 (2019) 116–143.
[13] A.S. Lilly, J.J. Thankamony, M. Wittmann, M. Kaushik, B. Corzilius, Dynamic nuclear polarization for sensitivity enhancement in modern solid-state NMR, Prog. Nucl. Magn. Reson. Spectrosc. 102–103 (2017) 120–195.
[14] C.F. Hwang, D.A. Hill, Phenomenological model for the new effect in dynamic polarization, Phys. Rev. Lett. 19 (1967) 1011–1014.
[15] K.-N. Hu, G.T. Debelouchina, A.A. Smith, R.G. Griffin, Quantum mechanical theory of dynamic nuclear polarization in solid dielectrics, J. Chem. Phys. 134 (2011) 125105–125119.
[16] Y. Hovav, A. Feintuch, S. Vega, Theoretical aspects of dynamic nuclear polarization in the solid state–the cross effect, J. Magn. Reson. 214 (2012) 29–41.
[17] K.R. Thurber, R. Tycko, Theory for cross effect dynamic nuclear polarization under magic-angle spinning in solid state nuclear magnetic resonance: The importance of level crossings, J. Chem. Phys. 137 (2012) 084508–084514.
[18] F. Mentink-Vigier, U. Akbey, H. Oschkinat, S. Vega, A. Feintuch, Theoretical aspects of magic angle spinning - dynamic nuclear polarization, J. Magn. Reson. 258 (2015) 102–120.
[19] A. Equbal, K. Tagami, S. Han, Balancing dipolar and exchange coupling in biradicals to maximize cross effect dynamic nuclear polarization, Phys. Chem. Chem. Phys. 22 (2020) 13569–13579.
[20] F. Mentink-Vigier, U. Akbey, Y. Hovav, S. Vega, H. Oschkinat, A. Feintuch, Fast passage dynamic nuclear polarization on rotating solids, J. Magn. Reson. 224 (2012) 13–21.
[21] F. Mentink-Vigier, S. Paul, D. Lee, A. Feintuch, S. Hediger, S. Vega, G. De Paepe, Nuclear depolarization and absolute sensitivity in magic-angle spinning cross effect dynamic nuclear polarization, Phys. Chem. Chem. Phys. 17 (2015) 21824–21836.
[22] Hediger, S.; Lee, D.; Mentink-Vigier, F.; De Paëpe, G., MAS-DNP Enhancements : Hyperpolarization, Depolarization, and Absolute Sensitivity. In *EPR Spectroscopy: Fundamentals and Methods*, Goldfarb, D.; Stoll, S., Eds. WILEY-VCH Verlag: 2018.
[23] K. Kundu, F. Mentink-Vigier, A. Feintuch, S. Vega, DNP Mechanisms, *EMagRes.* 8 (2019) 295–338.
[24] C. Ysacco, H. Karoui, G. Casano, F. Le Moigne, S. Combes, A. Rockenbauer, M. Rosay, W. Maas, O. Ouari, P. Tordo, Dinitroxides for Solid State Dynamic Nuclear Polarization, Appl. Magn. Reson. 43 (2012) 251–261.
[25] F. Mentink-Vigier, Optimizing nitroxide biradicals for cross-effect MAS-DNP: the role of g-tensors' distance, Phys. Chem. Chem. Phys. 22 (2020) 3643–3652.
[26] F. Mentink-Vigier, T. Dubroca, J. Van Tol, S.T. Sigurdsson, The distance between g-tensors of nitroxide biradicals governs MAS-DNP performance: The case of the bTurea family, J. Magn. Reson. 329 (2021) 107026.
[27] F.A. Perras, A. Sadow, M. Pruski, In Silico Design of DNP Polarizing Agents: Can Current Dinitroxides Be Improved?, ChemPhysChem 18 (2017) 2279–2287
[28] A.J. Rossini, C.M. Widdifield, A. Zagdoun, M. Lelli, M. Schwarzwälder, C. Copéret, A. Lesage, L. Emsley, Dynamic nuclear polarization enhanced NMR spectroscopy for pharmaceutical formulations, J. Am. Chem. Soc. 136 (2014) 2324–2334.
[29] N. Tiwari, S. Wi, F. Mentink-Vigier, N. Sinha, Mechanistic insights into the structural stability of collagen-containing biomaterials such as bones and cartilage, J. Phys. Chem. B 125 (18) (2021) 4757–4766.
[30] M. Hong, Solid-state dipolar INADEQUATE NMR spectroscopy with a large double-quantum spectral width, J. Magn. Reson. 136 (1) (1999) 86–91.
[31] X. Kang, A. Kirui, M.C.D. Widanage, F. Mentink-Vigier, D.J. Cosgrove, T. Wang, Lignin-polysaccharide interactions in plant secondary cell walls revealed by solid-state NMR, Nat. Commun. 10 (2019) 347.
[32] H. Takahashi, D. Lee, L. Dubois, M. Bardet, S. Hediger, G. De Paëpe, Rapid natural-abundance 2D 13C–13C correlation spectroscopy using dynamic nuclear polarization enhanced solid-state NMR and matrix-free sample preparation, Angew. Chem. Int. Ed. 51 (2012) 11766–11769.
[33] A.J. Rossini, A. Zagdoun, F. Hegner, M. Schwarzwälder, D. Gajan, C. Copéret, A. Lesage, L. Emsley, Dynamic nuclear polarization NMR spectroscopy of microcrystalline solids, J. Am. Chem. Soc. 134 (40) (2012) 16899–16908.
[34] W.Y. Chow, B.P. Norman, N.B. Roberts, L.R. Ranganath, C. Teutloff, R. Bittl, M.J. Duer, J.A. Gallagher, H. Oschkinat, Pigmentation chemistry and radical-based collagen degradation in alkaptonuria and osteoarthritic cartilage, Angew. Chem. Int. Ed. 59 (2020).
[35] G. Mollica, M. Dekhil, F. Ziarelli, P. Thureau, S. Viel, Quantitative structural constraints for organic powders at natural isotopic abundance using dynamic nuclear polarization solid-state NMR spectroscopy, Angew. Chem. Int. Ed. 54 (2015) 6028–6031.
[36] Y. Geiger, H.E. Gottlieb, Ü. Akbey, H. Oschkinat, G. Goobes, Studying the conformation of a Silaffin-derived pentalysine peptide embedded in bioinspired silica using solution and dynamic nuclear polarization magic-angle spinning NMR, J. Am. Chem. Soc. 138 (2016) 5561–5567.

[37] K. Märker, S. Paul, C. Fernández-de-Alba, D. Lee, J.-M. Mouesca, S. Hediger, G. De Paëpe, Welcoming natural isotopic abundance in solid-state NMR: probing π-stacking and supramolecular structure of organic nanoassemblies using DNP, Chem. Sci. 8 (2017) 974–987.
[38] K. Märker, M. Pingret, J.-M. Mouesca, D. Gasparutto, S. Hediger, G. De Paëpe, A new tool for NMR crystallography: complete 13C/15N assignment of organic molecules at natural isotopic abundance using DNP-enhanced solid-state NMR, J. Am. Chem. Soc. 137 (43) (2015) 13796–13799.
[39] T. Kobayashi, I.I. Slowing, M. Pruski, Measuring long-range 13C–13C correlations on a surface under natural abundance using dynamic nuclear polarization-enhanced solid-state nuclear magnetic resonance, J. Phys. Chem. C 121 (2017) 24687–24691.
[40] N.M. Szeverenyi, M.J. Sullivan, G.E. Maciel, Observation of spin exchange by two-dimensional fourier transform 13C cross polarization-magic-angle spinning, J. Magn. Reson. 47 (1982) 462–475.
[41] B.H. Meier, Polarization transfer and spin diffusion in solid state NMR, Academic Press: New York 18 (1994).
[42] A. Grommek, B.H. Meier, M. Ernst, Distance information from proton-driven spin diffusion under MAS, Chem. Phys. Lett. 427 (2006) 404–409.
[43] K. Takegoshi, S. Nakamura, T. Terao, 13C–1H dipolar-assisted rotational resonance in magic-angle spinning NMR, Chem. Phys. Lett. 344 (5–6) (2001) 631–637.
[44] K. Takegoshi, S. Nakamura, T. Terao, C-13-H-1 dipolar-driven C-13-C-13 recoupling without C-13 rf irradiation in nuclear magnetic resonance of rotating solids, J. Chem. Phys. 118 (5) (2003) 2325–2341.
[45] M. Weingarth, G. Bodenhausen, P. Tekely, Broadband magnetization transfer using moderate radio-frequency fields for NMR with very high static fields and spinning speeds, Chem. Phys. Lett. 488 (1–3) (2010) 10–16.
[46] B. Hu, O. Lafon, J. Trébosc, Q. Chen, J.-P. Amoureux, Broad-band homo-nuclear correlations assisted by 1H irradiation for bio-molecules in very high magnetic field at fast and ultra-fast MAS frequencies, J. Magn. Reson. 212 (2) (2011) 320–329.
[47] B. Hu, J. Trébosc, O. Lafon, Q. Chen, Y. Masuda, K. Takegoshi, J.-P. Amoureux, Very-long-distance correlations in proteins revealed by solid-state NMR spectroscopy, ChemPhysChem 13 (16) (2012) 3585–3588.
[48] G. Hou, S. Yan, S. Sun, Y. Han, I.-J.-L. Byeon, J. Ahn, J. Concel, A. Samoson, A.M. Gronenborn, T. Polenova, Spin diffusion driven by R-symmetry sequences: applications to homonuclear correlation spectroscopy in MAS NMR of biological and organic solids, J. Am. Chem. Soc. 133 (11) (2011) 3943–3953.
[49] S. Wi, L. Frydman, An efficient, robust new scheme for establishing broadband homonuclear correlations in biomolecular solid state NMR, Chemphyschem 21 (4) (2020) 284–294.
[50] M. Rance, O.W. Sørensen, G. Bodenhausen, G. Wagner, R.R. Ernst, K. Wüthrich, Improved spectral resolution in COSY 1H NMR spectra of proteins via double quantum filtering, Biochem. Biophys. Res. Commun. 117 (1983) 479–485.
[51] U. Piantini, O.W. Sorensen, R.R. Ernst, Multiple quantum filters for elucidating NMR coupling networks, J. Am. Chem. Soc. 104 (24) (1982) 6800–6801.
[52] A.J. Shaka, R. Freeman, Simplification of NMR spectra by filtration through multiple-quantum coherence, J. Magn. Reson. 51 (1) (1983) 169–173.
[53] J.J. Lopez, C. Kaiser, S. Shastri, C. Glaubitz, Double quantum filtering homonuclear MAS NMR correlation spectra: a tool for membrane protein studies, Journal of Biomolecular Nmr 41 (2) (2008) 97–104.
[54] M.R. Elkins, I.V. Sergeyev, M. Hong, Determining cholesterol binding to membrane proteins by cholesterol C-13 labeling in yeast and dynamic nuclear polarization NMR, J. Am. Chem. Soc. 140 (45) (2018) 15437–15449.
[55] M.J. Bayro, M. Huber, R. Ramachandran, T.C. Davenport, B.H. Meier, M. Ernst, R. G. Griffin, Dipolar truncation in magic-angle spinning NMR recoupling experiments, J. Chem. Phys. 130 (2009) 114506.
[56] F. Mentink-Vigier, I. Marin-Montesinos, A.P. Jagtap, T. Halbritter, J. van Tol, S. Hediger, D. Lee, S.T. Sigurdsson, G. De Paëpe, Computationally assisted design of polarizing agents for dynamic nuclear polarization enhanced NMR: The AsymPol Family, J. Am. Chem. Soc. 140 (2018) 11013–11019.
[57] F. Mentink-Vigier, S. Vega, G. De Paepe, Fast and accurate MAS–DNP simulations of large spin ensembles, Phys. Chem. Chem. Phys. 19 (2017) 3506–3522.
[58] M. Hohwy, C.M. Rienstra, C.P. Jaroniec, R.G. Griffin, Fivefold symmetric homonuclear dipolar recoupling in rotating solids: Application to double quantum spectroscopy, J. Chem. Phys. 110 (16) (1999) 7983.
[59] M. Rosay, M. Blank, F. Engelke, Instrumentation for solid-state dynamic nuclear polarization with magic angle spinning NMR, J. Magn. Reson. 264 (2016) 88–98.
[60] T. Dubroca, A.N. Smith, K.J. Pike, S. Froud, R. Wylde, B. Trociewitz, J.E. McKay, F. Mentink-Vigier, J. van Tol, S. Wi, W.W. Brey, J.R. Long, L. Frydman, S. Hill, A quasi-optical and corrugated waveguide microwave transmission system for simultaneous dynamic nuclear polarization NMR on two separate 14.1 T spectrometers, J. Magn. Reson. 289 (2018) 35–44.
[61] A. Pines, M.G. Gibby, J.S. Waugh, Proton-enhanced NMR of dilute spins in solids, J. Chem. Phys. 59 (1973) 569.
[62] E.O. Stejskal, J. Schaefer, J.S. Waugh, Magic-angle spinning and polarization transfer in proton-enhanced NMR, J. Magn. Reson. 28 (1) (1977) 105–112.
[63] B.M. Fung, A.K. Khitrin, K. Ermolaev, An improved broadband decoupling sequence for liquid crystals and solids, J. Magn. Reson. 142 (2000) 97–101.
[64] https://www.uniprot.org/uniprot/P02453.
[65] L. Ren, P. Yang, J. Zhang, C. Ding, P. Shang, Biomechanical and biophysical environment of bone from the macroscopic to the pericellular and molecular level, J. Mech. Behav. Biomed. Mater 50 (2015) 104–122.
[66] M. Unal, A. Creecy, J.S. Nyman, The role of matrix composition in the mechanical behavior of bone, Curr. Osteoporos Rep. 16 (3) (2018) 205–215.
[67] W.Y. Chow, R. Rajan, K.H. Muller, D.G. Reid, J.N. Skepper, W.C. Wong, R.A. Brooks, M. Green, D. Bihan, R.W. Farndale, D.A. Slatter, C.M. Shanahan, M.J. Duer, NMR spectroscopy of native and in vitro tissues implicates polyADP ribose in biomineralization, Science 344 (6185) (2014) 742–746.
[68] J.M. Courtney, C.M. Rienstra, Efficient dipolar double quantum filtering under magic angle spinning without a H-1 decoupling field, J. Magn. Reson. 269 (2016) 152–156.
[69] C. Sauvée, G. Casano, S. Abel, A. Rockenbauer, D. Akhmetzyanov, H. Karoui, D. Siri, F. Aussenac, W. Maas, R.T. Weber, T. Prisner, M. Rosay, P. Tordo, O. Quari, Tailoring of polarizing agents in the BTurea series for cross-effect dynamic nuclear polarization in aqueous media, Chem. Eur. J. 22 (2016) 5598–5606.
[70] A.P. Jagtap, M.A. Geiger, D. Stöppler, M. Orwick-Rydmark, H. Oschkinat, S.T. Sigurdsson, BcTol: A highly water-soluble biradical for efficient dynamic nuclear polarization of biomolecules, Chem. Commun. 52 (2016) 7020–7023.
[71] M.-A. Geiger, A.P. Jagtap, M. Kaushik, H. Sun, D. Stöppler, S.T. Sigurdsson, B. Corzilius, H. Oschkinat, Efficiency of water-soluble nitroxide biradicals for dynamic nuclear polarization in rotating solids at 9.4 T: BcTol-M and Cyolyl-TOTAPOL as new polarizing agents, Chem. Eur. J. 24 (2018) 13485–13494.
[72] D. Daube, M. Vogel, B. Suess, B. Corzilius, Dynamic nuclear polarization on a hybridized hammerhead ribozyme: An explorative study of RNA folding and direct DNP with a paramagnetic metal ion cofactor, Solid State Nucl. Magn. Reson. 101 (2019) 21–30.